Article

*Discovery Medicine* 2026; 38(204): 60–74
https://doi.org/10.24976/Discov.Med.202638204.5

# The Role of Ferroptosis in LPS-Induced Acute Lung Injury and the Synergistic Inhibition by Metallothionein-1 and VDPS

Ningfeng Dai[1], Nengfu Chen[1], Xiongfeng Pan[1], Minguo Chen[1], Tianwei Wang[2], Kai Lin[1,*]

[1]Department of Thoracic Surgery, The People's Hospital of Cangnan, 325800 Wenzhou, Zhejiang, China
[2]Department of Children's Rehabilitation, Ruian People's Hospital, 325200 Wenzhou, Zhejiang, China
*Correspondence: lkkl13145212025@163.com (Kai Lin)
Submitted: 18 October 2025 Revised: 12 December 2025 Accepted: 24 December 2025 Published: 20 January 2026

**Background: Acute lung injury (ALI) and its severe manifestation, acute respiratory distress syndrome, are life-threatening pulmonary disorders for which effective therapeutic interventions are currently lacking. This study aimed to investigate the role of ferroptosis in LPS-induced ALI and elucidate the synergistic mechanism of metallothionein-1 (MT-1) and galactoxylan polysaccharide (VDPS) in inhibiting ferroptosis, potentially offering novel therapeutic strategies for ALI.**

**Methods: Using Lipopolysaccharide (LPS)-induced murine models and MLE-12 cell lines, we analyzed ferroptosis-related indicators, including glutathione peroxidase 4 (GPX4), malondialdehyde (MDA), reduced glutathione (GSH), and iron content. Interventions with ferroptosis inhibitor ferrostatin-1 (Fer-1), activator erastin, and VDPS were performed. MT-1 knockdown experiments were conducted to explore its role in oxidative stress, iron metabolism, and inflammatory responses.**

**Results: LPS stimulation induced characteristic ferroptosis features in both mice and MLE-12 cells, manifested by increased pulmonary iron content, decreased GSH levels, elevated MDA levels, and reduced GPX4 expression ($p < 0.05$). Fer-1 treatment significantly ameliorated these oxidative stress markers and protected lung function ($p < 0.05$). LPS markedly upregulated MT-1 expression, while MT-1 knockdown exacerbated oxidative stress, lipid peroxidation, and ferroptosis ($p < 0.05$). VDPS effectively inhibited LPS-induced ferroptosis, reducing oxidative damage and inflammation ($p < 0.05$). Combined treatment with Fer-1 notably decreased pulmonary edema, inflammatory infiltration, and fibrosis ($p < 0.05$). VDPS also regulated iron metabolism, suppressing elevated iron levels in lung tissue and serum ($p < 0.05$). Importantly, MT-1 enhanced VDPS-mediated GPX4 pathway activation, synergistically inhibiting ferroptosis and attenuating LPS-induced oxidative injury ($p < 0.05$).**

**Conclusion: This study reveals the crucial role of ferroptosis in LPS-induced ALI. MT-1 enhances VDPS-mediated ferroptosis inhibition by modulating oxidative stress responses and antioxidant enzyme activities, effectively alleviating lung injury. These findings provide experimental evidence for MT-1 and VDPS as potential therapeutic strategies, highlighting the promising application of anti-ferroptosis therapy in ALI treatment.**

**Keywords:** acute lung injury; ferroptosis; MT-1; VDPS; LPS

## Introduction

Acute lung injury (ALI) and acute respiratory distress syndrome (ARDS) are common clinical syndromes characterized by extensive and rapid damage to the alveolar epithelium, pulmonary microvascular endothelium, and interstitial tissue of the lungs. These pathological alterations, triggered by various pulmonary or extrapulmonary insults, ultimately contribute to the continuous deterioration of respiratory function and the development of respiratory failure. Severe cases may progress to varying degrees of end-stage pulmonary changes [1,2]. While the pathogenesis of ALI remains incompletely understood, uncontrolled inflammation and oxidative stress are widely recognized as primary mechanisms [3]. Lipopolysaccharide (LPS), an essential structural molecule found in the outer membrane of gram-negative bacteria, is critically involved in the development of ALI and ARDS. It contributes to disease progression primarily by significantly increasing the permeability of the alveolar epithelial barrier and compromising the structural and functional integrity of lung tissue [4]. Previous research has revealed that exposure to LPS can trigger a variety of regulated cell death pathways, such as apoptosis, autophagy, pyroptosis, and necroptosis, reflecting its extensive impact on cellular survival and homeostasis; however, inhibiting these death pathways only partially alleviates LPS-induced lung tissue damage [5]. Current ALI/ARDS treatment primarily relies on various mechanical ventilation support strategies, yet no specific pharmacological interventions exist to significantly reduce mortality or improve quality of life [6]. Therefore, elucidating novel inflammatory mechanisms and exploring potential therapeutic targets for ALI/ARDS holds critical significance.

Ferroptosis represents a unique type of regulated cell death that arises from overwhelming lipid peroxidation within cellular membranes. This process exhibits distinct morphological and molecular characteristics that clearly differentiate it from other well-known modes of programmed cell death [7]. Recent research has increasingly demonstrated that ferroptosis is closely linked to a range of lung disorders, such as ALI and ARDS, pulmonary fibrosis, chronic obstructive pulmonary disease, as well as lung cancer [8–11]. Multiple studies utilizing ferroptosis inhibitors or transgenic animal models have demonstrated the crucial role of ferroptosis in ALI. Liu *et al*. [12] found that ferroptosis participates in LPS-induced inflammatory responses, and treatment with the ferroptosis inhibitor ferrostatin-1 (Fer-1) significantly ameliorated alveolar epithelial inflammatory damage in ALI mice. These findings indicate that ferroptosis inhibition may represent an important therapeutic breakthrough for ALI. However, research on ferroptosis in ALI remains in preliminary stages, and the specific molecular regulatory mechanisms linking ferroptosis to ALI pathogenesis require further investigation.

Metallothionein-1 (MT-1) is a metal-binding and antioxidant protein characterized by low molecular weight and high cysteine content with diverse biological functions [13–15]. Previous research has demonstrated that MT-1 is widely expressed in a variety of tissues throughout the body and, as an important stress-responsive protein, its upregulation confers protection in various disease models through regulation of metal homeostasis, oxidative stress, and inflammation. Multiple stress factors including LPS, heavy metals, and dexamethasone can induce MT-1 expression and enhance its activity [13,16]. Recent evidence suggests that MT-1 functions as an important molecular regulator of ferroptosis, whereby its functional suppression or loss amplifies lipid peroxidation-driven cell death, while its transcriptional induction exerts a potent cytoprotective effect against ferroptotic injury [17,18]. Another study demonstrated that MT-1, as a zinc-inducible cytoprotective protein, plays a pivotal role in mitigating pulmonary injury by maintaining zinc homeostasis, restraining neutrophil overactivation, and attenuating inflammatory oxidative damage within the lung microenvironment [19]. Given MT-1's properties in reactive oxygen species (ROS) scavenging, antioxidant defense, and inflammatory suppression, it may serve as a crucial regulatory molecule in ALI and ferroptosis, potentially representing an effective therapeutic target. In-depth investigation of its regulatory mechanisms could provide new therapeutic perspectives for ALI. Therefore, this study developed cellular and animal models of ALI to investigate the role of MT-1 in ALI and elucidate its molecular regulatory mechanisms, with a particular focus on the involvement of ferroptosis in ALI pathogenesis and its regulatory relationship with MT-1. Additionally, we employed siRNA-mediated *MT-1* gene silencing in MLE-12 cells to examine changes in downstream signaling pathway proteins, thereby exploring MT-1's role and mechanisms in LPS-induced ALI.

*Viola diffusa*, a herbaceous plant belonging to the Violaceae family, has been traditionally used to treat hepatitis, pleurisy, conjunctivitis, venomous snake bites, and ulcerative carbuncles [20]. To date, its chemical constituents have not been systematically studied. In our previous research, we isolated and identified a novel galactoxylan polysaccharide (VDPS) from *Viola diffusa*, primarily composed of Rha, GlcA, Glc, Gal, Xyl, and Fuc, with a molecular weight of $2.72 \times 10^3$ kDa, which demonstrated protective effects against LPS-induced ALI [21]. Given the similarities between MT-1 and VDPS in antioxidant stress response and inflammatory inhibition, we hypothesize that MT-1 may synergistically enhance VDPS-mediated ferroptosis inhibition, thereby augmenting protection against ALI. This investigation aims to identify novel therapeutic targets and inform the development of effective treatments for ALI.

## Materials and Methods

### *Experimental Animals and Model Establishment*

Healthy male C57BL/6 mice (6–8 weeks old, 21–24 g) were purchased from Beijing Vital River Laboratory Animal Technology Co., Ltd (China). All experimental procedures were performed in adherence to the institutional animal ethics guidelines. The mice were maintained under controlled conditions (temperature $22 \pm 2$ °C, humidity $55\% \pm 5\%$, 12/12 h light/dark cycle) with *ad libitum* access to food and water.

To establish the LPS-induced ALI model, the mice were deprived of water for 4 h prior to experimentation. Anesthesia was induced with 0.4% sodium pentobarbital (Sigma-Aldrich, Cat# P3761, St. Louis, MO, USA). After anesthesia, the trachea was surgically exposed, and LPS was administered intratracheally at a dose of 5 mg/kg (Sigma-Aldrich, Cat# L2630, St. Louis, MO, USA) [22]. The mice were gently rotated to ensure uniform distribution of the solution and then placed in the lateral position. After recovery, animals were returned to the facility for monitoring.

VDPS extraction and physicochemical characterization were conducted as described in our previous study [21]. VDPS (200 mg/kg) was administered by oral gavage once daily for 7 consecutive days prior to ALI induction. Ferroptosis-related interventions were performed 2 h before LPS challenge: Erastin (10 mg/kg, MedChemExpress, Cat# HY-15763, Monmouth Junction, NJ, USA) and Fer-1 (0.8 mg/kg, MedChemExpress, Cat# HY-100579, Monmouth Junction, NJ, USA) were administered intraperitoneally.

At 72 h post-LPS administration, the mice were anesthetized by intraperitoneal injection of sodium pentobarbital (200 mg/kg, Sigma-Aldrich, Cat# P3761, St. Louis, MO, USA) and subsequently euthanized by cervical dislocation. For further analysis, lung specimens and bronchoalveolar lavage fluid (BALF) were collected.

### *HE Staining and Histological Scoring*

Fixed lung tissues underwent gradient dehydration using ethanol series, followed by clearing in xylene and staining with hematoxylin-eosin (HE) staining kit (Beyotime, Cat# C0105, Shanghai, China) for histological analysis. Pathological sections were examined under a light microscope (Leica DM2000, Leica Microsystems, Wetzlar, Germany) to evaluate inflammatory cell infiltration, edema, and tissue damage.

Lung injury was scored according to the criteria described by Matute-Bello *et al.* [23], based on five histopathological parameters: alveolar interstitial edema, congestion, patchy hemorrhage, neutrophil infiltration, and alveolar wall thickening or hyaline membrane formation. Each parameter was graded on a five-point scale from 0 to 4, representing minimal (0), mild (1), moderate (2), severe (3), and extreme (4) injury, and the total lung injury score was calculated as the sum of the individual scores. All scoring was performed independently by two blinded pathologists to ensure objectivity and reduce subjective bias.

### *Masson's Trichrome Staining*

Sections were deparaffinized, rehydrated through graded ethanol, and stained using a Masson's Trichrome Staining Kit (Beyotime, Cat# G1340, Shanghai, China) according to the manufacturer's instructions. Finally, the sections were dehydrated, cleared in xylene, and observed under a light microscope (Olympus, Model BX53, Tokyo, Japan).

### *BALF Collection*

Following 72 hours of LPS treatment, the mice were administered pentobarbital via intraperitoneal injection and subsequently subjected to bronchoalveolar lavage. The trachea was punctured with a blunt-end, sterile, 22-gauge needle. The lungs were lavaged twice with 0.8 mL of normal saline in a slow and uniform manner, and the resulting lavage solution was collected. A BCA kit (Beyotime, Cat# P0010, Shanghai, China) was used to measure the total protein concentration of BALF.

### *ELISA*

Serum and BALF concentrations of tumor necrosis factor $\alpha$ (TNF-$\alpha$), interleukin (IL)-1$\beta$, and IL-6 were measured using ELISA kits (Beyotime, TNF-$\alpha$: Cat# PT512, IL-1$\beta$: Cat# PI301, IL-6: Cat# PI326, Shanghai, China).

### *Detection of Iron Level*

Tissue samples were homogenized in 9 volumes of physiological saline (w/v = 1:9) on ice, and both tissue homogenates and blood samples were centrifuged at 2500 rpm for 10 minutes at 4 °C to collect supernatants, which were stored at –80 °C until analysis. Iron levels in lung tissue and serum supernatants were determined using an Iron Assay Kit (Novus Biologicals, Cat#NBP3-25844, Littleton, CO, USA). Absorbance was measured at 532 nm using a microplate reader (Multiskan GO, Thermo Fisher Scientific, Waltham, MA, USA).

### *Detection of Malondialdehyde (MDA) Levels*

Tissue specimens were homogenized in 500 µL RIPA lysis buffer (Beyotime, Cat# P0013B, Shanghai, China) and lysed on ice for 30 minutes. Cell specimens were washed with phosphate-buffered saline (PBS; Beyotime, Cat# C0221, Shanghai, China) and lysed in 200 µL lysis buffer at 4 °C for 30 minutes. All samples were centrifuged at 12,000 rpm for 10 minutes, and protein concentration in supernatants was determined using the BCA protein assay kit (Beyotime, Cat# P0010, Shanghai, China). Serum samples were measured directly.

Following the malondialdehyde (MDA) Assay Kit's protocol (Beyotime, Cat# S0131, Shanghai, China), 200 µL of the supernatant was transferred to a microplate and absorbance was measured at 532 nm using a microplate reader (Multiskan GO, Thermo Fisher Scientific, Waltham, MA, USA), and the MDA content was subsequently calculated (expressed as µmol/mg).

### *Detection of Total GSH*

Tissue samples were rapidly frozen in liquid nitrogen and ground into a fine powder using a pre-cooled mortar and pestle. For every 10 mg of tissue, protein removal reagent from a Glutathione (GSH) assay kit (Nanjing Jiancheng Bioengineering Institute, Cat# A006-2-1, Nanjing, China) was added according to the manufacturer's instructions. After incubation and centrifugation, the supernatants were collected for GSH measurement. Cell samples were washed with PBS, scraped, and centrifuged. The resulting pellets underwent three freeze-thaw cycles in liquid nitrogen and were then processed using the same GSH assay kit. GSH levels in both tissue and cell samples were determined at 532 nm using a microplate reader (Multiskan GO, Thermo Fisher Scientific, Waltham, MA, USA).

### *Cell Culture*

Mouse lung epithelial MLE-12 cells (American Type Culture Collection, ATCC® CRL-2110™, Manassas, VA, USA) were cultured in Dulbecco's Modified Eagle Medium (DMEM; Gibco, Cat# 11965-092, Grand Island, NY, USA) supplemented with 10% fetal bovine serum (FBS; Gibco, Cat# 10099-141, Grand Island, NY, USA) and 1% penicillin–streptomycin solution (Beyotime, Cat# C0222, Shanghai, China) at 37 °C in a humidified incubator containing 5% $CO_2$. All cells were authenticated by short tandem repeat profiling and confirmed to be free of mycoplasma contamination.

### Cell Treatment

The siRNA sequences were synthesized by GeneCreate Bioengineering Co., Ltd. (Wuhan, China). The specific sequences were siMT-1: F: 5′-CCUCAAUGCGAUCA UAUAUUTT-3′, R: 5′-AUAUAUGAUCGAUUGA GGTT-3′ and siNC: F: 5′-UUCUCC GAACGUGUCACGUTT-3′, R: 5′-ACGUGACAC GUUCGGAGAATT-3′. MLE-12 cells were seeded in a 6-well plate at a density of $1 \times 10^5$ cells per well. Transfection was performed when cell confluence reached approximately 70%. Transfection complexes were prepared by mixing 200 µL serum-free DMEM, 50 nM siRNA, and 5 µL Lipofectamine™ 3000 transfection reagent (Invitrogen, Cat# L3000015, Carlsbad, CA, USA). The mixture was gently pipetted, incubated for 20 min at room temperature, and then added dropwise to 6-well plates for a 48-hour incubation period.

After transfection, cells were subjected to drug pretreatment. For combined pretreatment, VDPS (100 µg/mL) and/or Fer-1 (1 µM, MedChemExpress, Cat# HY-100579, Monmouth Junction, NJ, USA) or erastin (1 µM, MedChemExpress, Cat# HY-15763, Monmouth Junction, NJ, USA) were added simultaneously to serum-containing medium and incubated for 2 h. Following pretreatment, the medium containing the compounds was maintained, and cells were stimulated with LPS (20 mg/L, Sigma-Aldrich, Cat# L2630) for the indicated period to establish the inflammatory injury model. Control groups received either VDPS or vehicle treatment, as appropriate.

### Cell Viability Assay

Cell viability was assessed using the Cell Counting Kit-8 (CCK-8; Dojindo Laboratories, Cat# CK04, Kumamoto, Japan) according to the manufacturer's instructions. Cells were seeded in 96-well plates at a density of $1 \times 10^4$ cells/mL and allowed to adhere overnight in a humidified incubator (Heracell 150i, Thermo Fisher Scientific, Waltham, MA, USA). After treatment with the respective drugs for 24 hours, 10 µL of CCK-8 reagent was added to each well and incubated for 2 h at 37 °C. The optical density was then measured at 450 nm using a microplate reader (Multiskan GO, Thermo Fisher Scientific, Waltham, MA, USA).

### Detection of Cellular ROS

Cells were seeded in 6-well plates at a density of $1 \times 10^4$ cells/mL and treated as indicated. After treatment, cells were incubated with 10 µmol/L DCFH-DA (Beyotime, Cat# S0033S, Shanghai, China) for 20 minutes at 37 °C in the dark for intracellular ROS detection. Following three PBS washes to remove excess dye, fluorescence signals were observed and imaged under a fluorescence microscope (Leica DMi8, Leica Microsystems, Wetzlar, Germany).

### Western Blotting

Approximately 25 mg of lung tissue or collected cells were lysed in RIPA lysis buffer (Beyotime, Cat# P0013B, Shanghai, China) on ice for 30 minutes. Lysates were centrifuged at 12,000 rpm for 10 minutes at 4 °C, and protein concentration was determined using the BCA Protein Assay Kit (Thermo Fisher Scientific, Cat# 23225, Waltham, MA, USA). Equal amounts of protein were separated by SDS-PAGE using 10% polyacrylamide gels and transferred onto 0.45 µm PVDF membranes (Millipore, Cat# IPVH00010, Burlington, MA, USA). Membranes were blocked with 5% non-fat dry milk (BD Difco, Cat# 232100, Sparks, MD, USA) in Tris-buffered saline with Tween-20 (TBST) for 2 hours at room temperature, followed by incubation with specific primary antibodies (diluted 1:1000; anti-glutathione peroxidase 4 (GPX4) antibody, Cat# ab125066, Abcam, Cambridge, UK; anti-MT-1 antibody, Cat#NB018787, Novus Biologicals, Littleton, CO, USA; anti-SLC7A11 antibody, Cat# ab307601, Abcam, Cambridge, UK; anti-$\beta$-actin, Cat# ab8226, Abcam, Cambridge, UK) overnight at 4 °C. After washing, membranes were incubated with HRP-conjugated goat anti-rabbit and goat anti-mouse IgG secondary antibodies (diluted 1:5000; Beyotime, Cat# A0208 and A0216, Shanghai, China) at room temperature for 1 h. Protein bands were visualized using an enhanced chemiluminescence detection kit (Thermo Fisher Scientific, Cat# 32106, Waltham, MA, USA) and imaged using a ChemiDoc XRS+ Imaging System (Model 1708265, Bio-Rad, Hercules, CA, USA). Densitometric analysis of protein bands was performed using ImageJ software (National Institutes of Health, Version 1.53t, Bethesda, MD, USA). The relative protein expression levels were calculated as the ratio of the target protein band intensity to that of $\beta$-actin, and the results were normalized to the control group.

### Statistical Analysis

All data were analyzed using GraphPad Prism 8.3.0 (GraphPad Software, San Diego, CA, USA). Quantitative data are presented as mean ± standard deviation (SD) from at least three independent experiments or $n$ biological replicates as indicated in the figure legends. Data distribution was assessed for normality using the Shapiro–Wilk test and for homogeneity of variance using Levene's test. For comparisons between two groups, an unpaired Student's $t$-test was used. For comparisons involving three or more groups, one-way analysis of variance (ANOVA) was performed; when ANOVA indicated significance, Tukey's post-hoc test was used for all pairwise comparisons (or Dunnett's post-hoc test when multiple groups were compared only against a single control). A $p$ value $< 0.05$ was considered statistically significant.

## Results

### *Ferroptosis Mediates LPS-induced ALI in vivo and in vitro*

To investigate the involvement of ferroptosis in LPS-induced acute lung injury *in vivo*, we measured biochemical indicators of iron metabolism and oxidative stress in lung tissue and serum. As shown in Fig. 1A–H, LPS administration significantly increased iron levels in both lung tissue and serum ($p < 0.05$), accompanied by decreased GSH levels ($p < 0.001$), increased MDA production ($p < 0.001$), and reduced GPX4 expression ($p < 0.001$), indicating enhanced ferroptotic activity. Treatment with erastin further exacerbated these changes ($p < 0.05$), resulting in greater iron accumulation, more pronounced oxidative stress, and further suppression of GPX4. In contrast, Fer-1 pretreatment effectively alleviated LPS-induced ferroptotic alterations ($p < 0.05$), significantly reducing tissue and serum iron levels, restoring GSH levels, lowering MDA content, and increasing GPX4 expression. These results demonstrate that ferroptosis contributes to the progression of LPS-induced lung injury in mice, and Fer-1 exerts protective effects by inhibiting ferroptotic pathways.

To further confirm the activation of ferroptosis under *in vitro* conditions, MLE-12 cells were exposed to increasing concentrations of LPS (0, 1, 10, 20, 40, and 80 mg/L) in serum-free medium for 24 hours, and cell viability was assessed using the CCK-8 assay. As shown in Fig. 1I, 20 mg/L LPS significantly reduced cell viability ($p < 0.01$); therefore, this concentration was used for subsequent experiments. LPS stimulation decreased MLE-12 cell viability, which was further reduced by erastin treatment ($p < 0.05$), whereas Fer-1 significantly restored cell viability ($p < 0.05$) (Fig. 1J). Consistent with the *in vivo* findings, Fer-1 treatment in LPS-exposed MLE-12 cells markedly increased GPX4 protein expression, enhanced GSH levels, and reduced MDA levels ($p < 0.05$) (Fig. 1K–N), indicating effective attenuation of lipid peroxidation and ferroptotic stress. Collectively, these results suggest that LPS induces ferroptosis in lung tissue and epithelial cells, and Fer-1 mitigates ferroptotic cell death.

### *MT-1 Exerts Protective Effects in LPS-induced Ferroptosis by Regulating Oxidative Stress and Antioxidant Enzyme Activity*

To verify the effect of LPS-induced ALI on MT-1 protein expression in lung tissue, we examined MT-1 protein levels in LPS-induced mouse lungs. As shown in Fig. 2A,B, LPS treatment significantly increased MT-1 protein expression compared with the control group ($p < 0.05$). Co-treatment with erastin further enhanced MT-1 upregulation ($p < 0.001$), whereas Fer-1 pretreatment effectively attenuated MT-1 expression, restoring it toward baseline levels ($p < 0.05$), suggesting a protective role of Fer-1 in modulating ferroptosis-associated protein changes.

Consistent with the *in vivo* results, *in vitro* experiments in MLE-12 cells revealed that LPS exposure significantly increased MT-1 protein expression ($p < 0.001$). This upregulation was further potentiated by erastin ($p < 0.001$), while Fer-1 pretreatment significantly reduced MT-1 levels toward baseline ($p < 0.001$) (Fig. 2C,D). These observations were confirmed by immunofluorescence analysis (Fig. 2E,F).

To further investigate the regulatory role of MT-1 in LPS-induced ferroptosis-associated responses, MLE-12 cells were transfected with either siCont or siMT-1 and subsequently treated with PBS or LPS for 24 hours. As shown in Fig. 2G–K, MT-1 knockdown significantly decreased cell viability and GSH levels, and markedly increased MDA and ROS production ($p < 0.05$). Further examination of ferroptosis-related proteins revealed significant reductions in GPX4 and SLC7A11 expression in MT-1 knockdown cells ($p < 0.05$) (Fig. 2L–O). These results indicate that MT-1 knockdown enhances oxidative stress and lipid peroxidation while impairing antioxidant capacity and cell viability in lung epithelial cells, highlighting the protective role of MT-1 against LPS-induced ferroptotic injury.

### *VDPS Alleviates LPS-induced ALI by Inhibiting Ferroptosis*

The ALI mouse model was established via intratracheal administration of LPS at a dose of 5 mg/kg, as illustrated in the experimental workflow (Fig. 3A). Pretreatment with Fer-1 and VDPS effectively prevented the LPS-induced increase in lung tissue wet/dry (W/D) ratio, indicating attenuation of pulmonary edema ($p < 0.001$) (Fig. 3B). Subsequently, right lung weight and corresponding lung index were measured, and BALF analyses were performed to quantify both cellular components and total protein concentration, providing comprehensive indicators of pulmonary inflammation and injury severity. Results showed that the Fer-1 and VDPS pretreated groups exhibited significantly lower right lung weight and lung index compared to the LPS-only group ($p < 0.001$) (Fig. 3C,D). BALF analysis further demonstrated that Fer-1 and VDPS pretreatment markedly attenuated LPS-induced increases in total cell number and protein concentration, notably reducing inflammatory cell infiltration into the alveolar spaces ($p < 0.05$) (Fig. 3E–I).

Consistently, Fer-1 and VDPS pretreatment significantly suppressed LPS-induced systemic inflammation, as evidenced by reduced serum levels of TNF-$\alpha$, IL-1$\beta$, and IL-6 ($p < 0.05$) (Fig. 3J–L). Histological examination using HE staining revealed that LPS administration caused severe pathological changes in lung tissue, including thickened alveolar walls, alveolar collapse, disruption of normal structural integrity, edema and thickened alveolar septa, and extensive inflammatory cell infiltration ($p < 0.001$) (Fig. 3N). Compared with the LPS group, Fer-1 and VDPS pretreatment markedly mitigated lung dam-

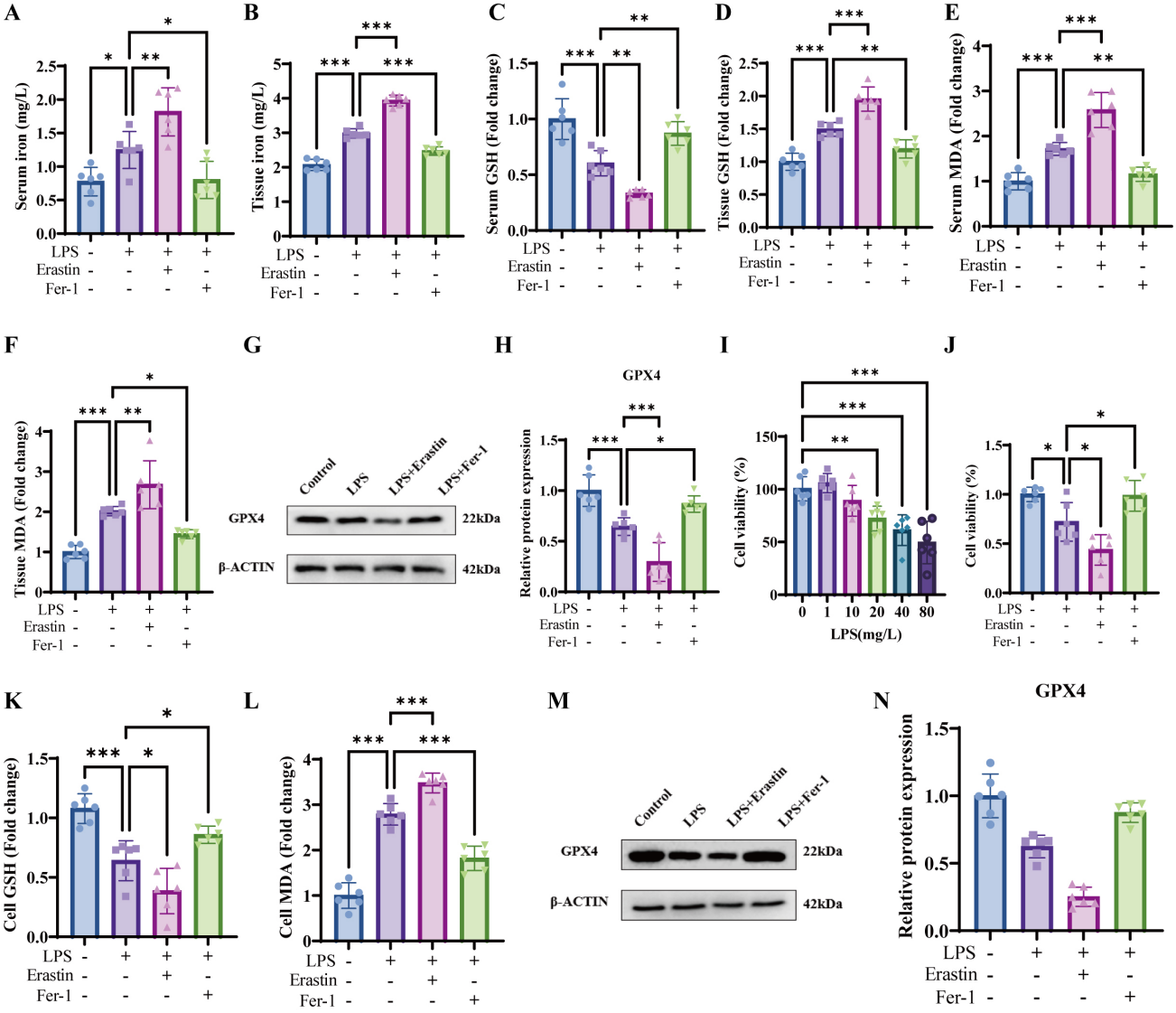


**Fig. 1. LPS-induced ALI affects lung tissue function through ferroptosis pathway.** (A) Serum iron levels in ALI mice. (B) Lung tissue iron levels in ALI mice. (C) Serum GSH levels in ALI mice. (D) Lung tissue GSH levels in ALI mice. (E) Serum MDA levels in ALI mice. (F) Lung tissue MDA levels in ALI mice. (G,H) GPX4 protein expression in ALI mouse lung tissue. (I) Cell viability of MLE-12 cells at 24 hours after LPS stimulation. (J) Effects of different treatments on LPS-treated MLE-12 cell viability. (K) Effects of different treatments on GSH levels in LPS-treated MLE-12 cells. (L) Effects of different treatments on MDA levels in LPS-treated MLE-12 cells. (M,N) Effects of different treatments on GPX4 protein expression in LPS-treated MLE-12 cells ($n = 6$, *$p < 0.05$, **$p < 0.01$, ***$p < 0.001$). Abbreviations: ALI, Acute lung injury; GSH, Reduced glutathione; GPX4, Glutathione peroxidase 4; LPS, Lipopolysaccharide; MDA, Malondialdehyde.

age, resulting in significantly lower lung injury scores ($p < 0.001$) (Fig. 3M,N). Masson's trichrome staining further demonstrated that Fer-1 and VDPS pretreatment significantly reduced LPS-induced pulmonary interstitial fibrosis (Fig. 3O,P). Finally, assessment of 72-hour survival in septic ALI mice indicated that Fer-1 and VDPS pretreatment significantly improved survival rates at 72 h post-treatment ($p < 0.05$) (Fig. 3Q).

Furthermore, we assessed the levels of GSH and MDA in both serum and lung tissue. The results indicated that, in comparison with the LPS group, mice treated with Fer-1 and VDPS exhibited a significant reduction in MDA concentrations, reflecting decreased lipid peroxidation in systemic circulation and pulmonary tissue ($p < 0.05$) (Fig. 4A,B), while GSH levels was significantly elevated ($p < 0.01$) (Fig. 4C,D). To gain deeper insight into alterations in iron homeostasis, we quantified iron concentrations in both lung tissue and serum, providing a detailed assessment of systemic and pulmonary iron metabolism under experimental conditions. Twenty-four hours following intratracheal administration of LPS, the total iron concentrations in both lung tissue and serum were markedly increased,

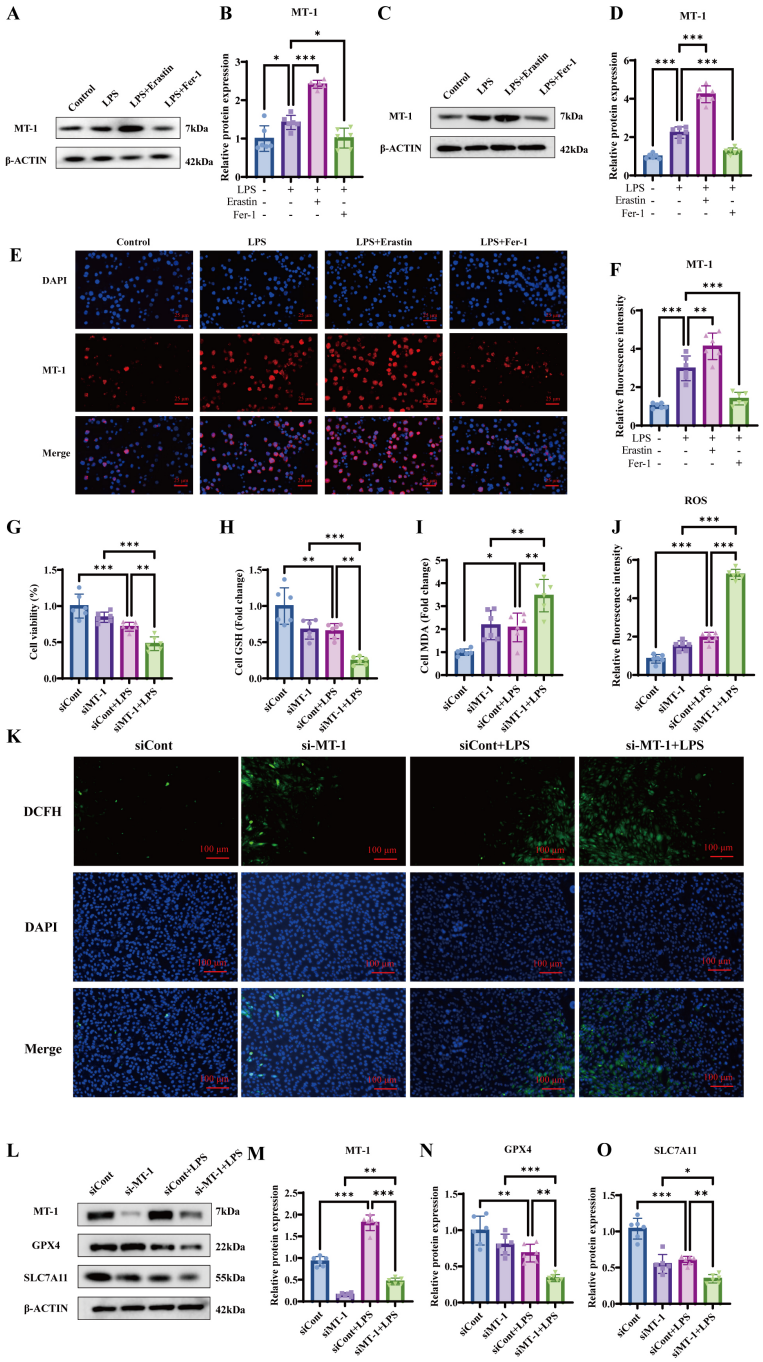


**Fig. 2. MT-1 exerts protective effects in LPS-induced ferroptosis by regulating oxidative stress and antioxidant enzyme activity.** (A) MT-1 protein expression levels in lung tissue. (B) Quantitative analysis of MT-1 protein expression in lung tissue. (C) MT-1 protein expression levels in MLE-12 cells. (D) Quantitative analysis of MT-1 protein expression in MLE-12 cells. (E) Immunofluorescence detection of MT-1 expression in MLE-12 cells under different treatments; red fluorescence represents MT-1 protein, blue fluorescence indicates nuclei (scale bar: 100 μm, magnification 100×). (F) Statistical analysis of relative immunofluorescence intensity. (G) Cell viability of MLE-12 cells under different treatments. (H) GSH levels in MLE-12 cells under different treatments. (I) MDA content in MLE-12 cells under different treatments. (J) Statistical analysis of ROS levels in each group. (K) ROS levels in MLE-12 cells detected by fluorescent probe DCFH-DA; green fluorescence represents ROS (scale bar: 50 μm, magnification 200×). (L) Expression of ferroptosis-related proteins. (M) Quantitative analysis of MT-1 protein expression. (N) Quantitative analysis of GPX4 protein expression. (O) Quantitative analysis of SLC7A11 protein expression ($n = 6$, *$p < 0.05$, **$p < 0.01$, ***$p < 0.001$). Abbreviations: GSH, Reduced glutathione; GPX4, Glutathione peroxidase 4; LPS, Lipopolysaccharide; MDA, Malondialdehyde; MT-1, Metallothionein-1; ROS, Reactive oxygen species.

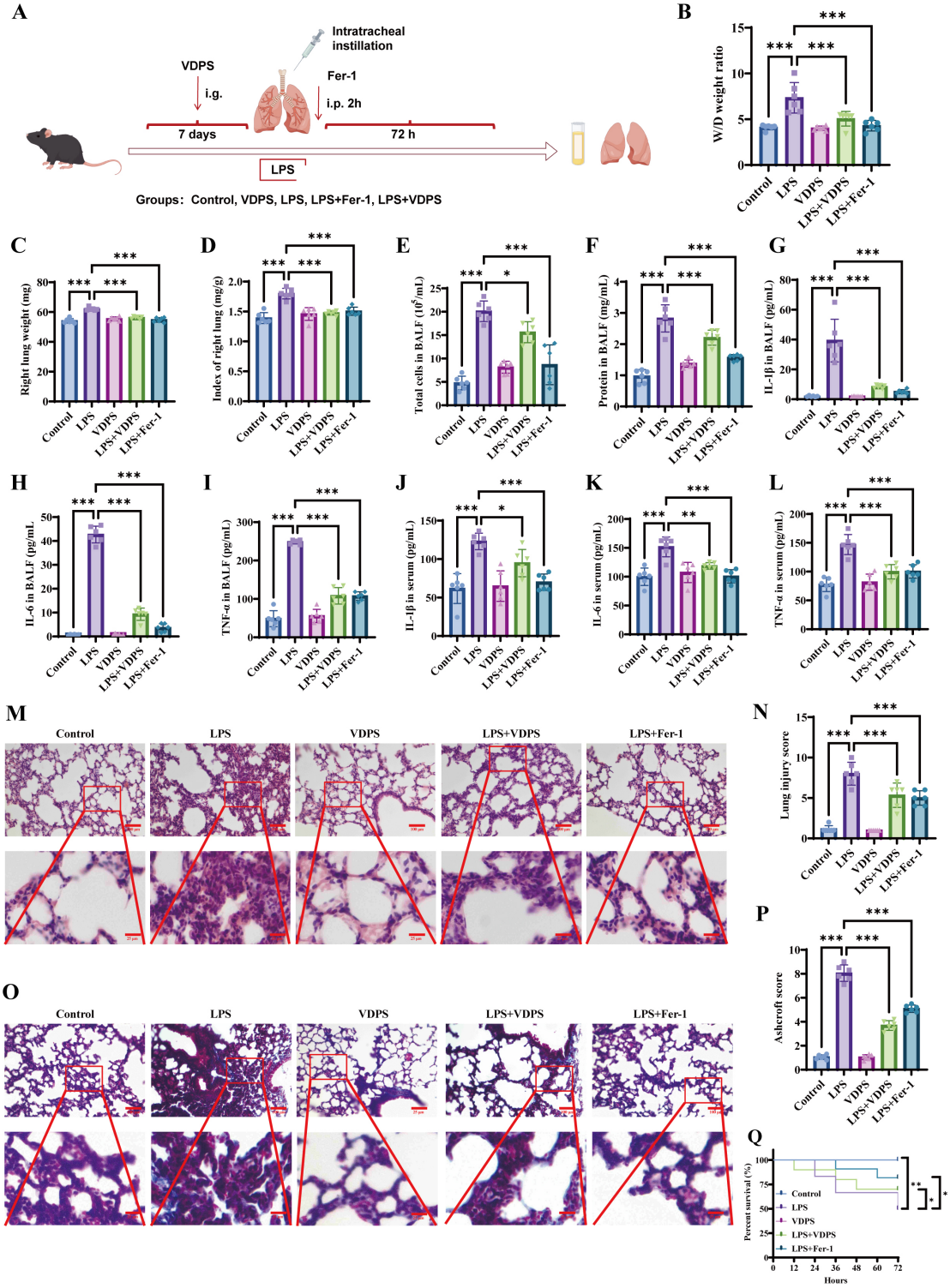


**Fig. 3. Protective effects of VDPS in ALI mice.** (A) Experimental workflow diagram (Created with Figdraw). (B) Lung tissue wet/dry (W/D) ratio. (C) Right lung weight in mice. (D) Right lung index in mice. (E) Total cell count in BALF. (F) Protein content in BALF. (G–I) IL-1$\beta$, IL-6, and TNF-$\alpha$ content in BALF. (J–L) Serum IL-1$\beta$, IL-6, and TNF-$\alpha$ content. (M) HE staining of lung tissue (scale bar: 100 µm, magnification 200×; 25 µm, magnification 400×). (N) Mouse lung injury score. (O) Masson's trichrome staining of lung tissue (scale bar: 100 µm, magnification 200×; 25 µm, magnification 400×). (P) Ashcroft score of the mice. (Q) 72-hour post-treatment survival analysis of mice ($n$ = 6, *$p < 0.05$, **$p < 0.01$, ***$p < 0.001$). Abbreviations: BALF, Bronchoalveolar lavage fluid; HE, Hematoxylin-eosin; IL, Interleukin; LPS, Lipopolysaccharide; TNF-$\alpha$, Tumor necrosis factor $\alpha$.

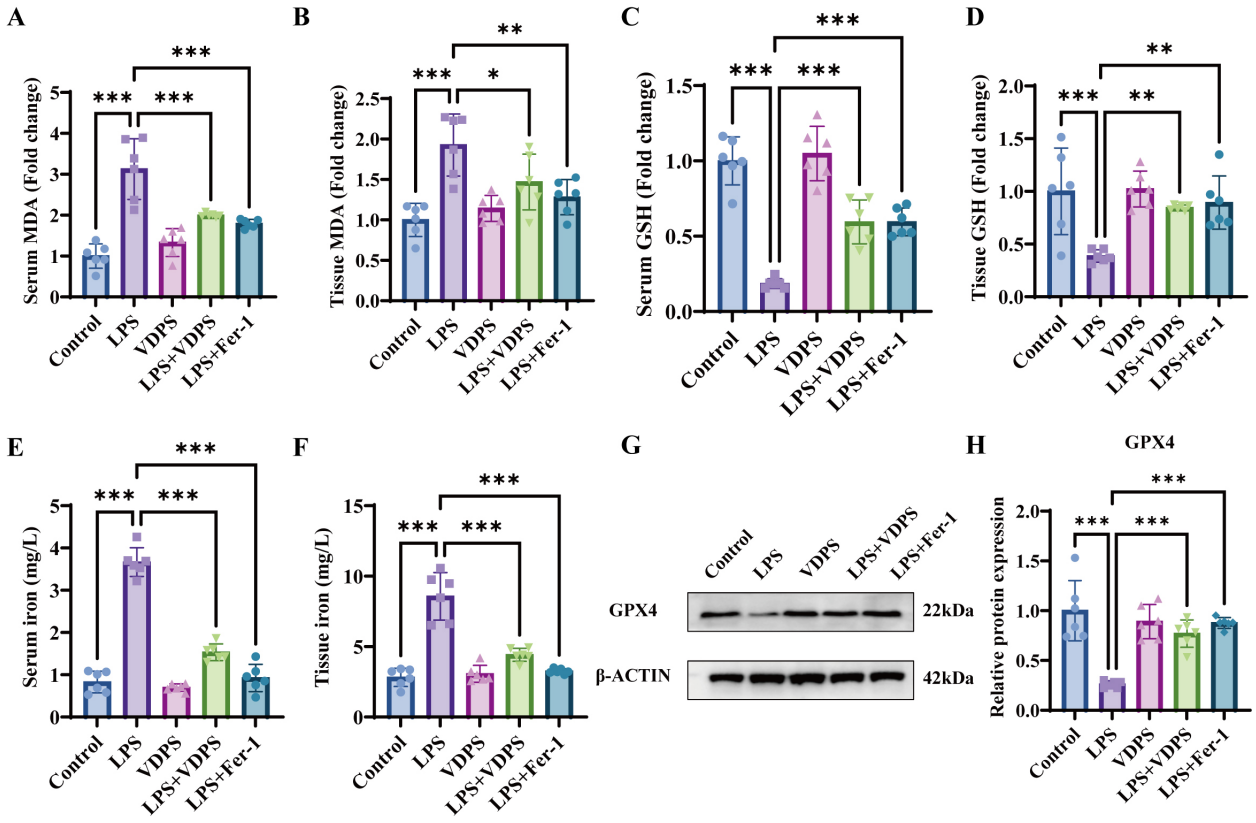


**Fig. 4. VDPS alleviates LPS-induced ALI by inhibiting ferroptosis and oxidative stress.** (A) Changes in serum MDA levels in ALI mice. (B) Changes in lung tissue MDA levels in ALI mice. (C) Changes in serum GSH levels in ALI mice. (D) Changes in lung tissue GSH levels in ALI mice. (E) Changes in serum iron levels in ALI mice. (F) Changes in lung tissue iron levels in ALI mice. (G) Western blot analysis of GPX4 protein expression. (H) Quantitative analysis of GPX4 protein expression ($n = 6$, *$p < 0.05$, **$p < 0.01$, ***$p < 0.001$). Abbreviations: ALI, Acute lung injury; GSH, Reduced glutathione; GPX4, Glutathione peroxidase 4; LPS, Lipopolysaccharide; MDA, Malondialdehyde.

indicating a substantial disruption of iron homeostasis associated with LPS-induced pulmonary injury, while Fer-1 and VDPS pretreatment significantly suppressed this elevation ($p < 0.001$) (Fig. 4E,F). Western blot analysis revealed that Fer-1 and VDPS pretreatment markedly increased expression of the ferroptosis marker GPX4, showing significant upregulation compared to the LPS group ($p < 0.001$) (Fig. 4G,H). In summary, the present study provides evidence that VDPS effectively mitigates LPS-induced ALI through multiple mechanisms, including the inhibition of ferroptotic cell death, attenuation of oxidative stress, modulation of inflammatory responses, and regulation of iron metabolism, highlighting its potential as a therapeutic agent for ALI.

### *VDPS Inhibits Lipid Peroxidation and Ferroptosis in MLE-12 Cells*

To investigate whether VDPS can inhibit ferroptosis *in vitro*, we developed a cellular injury model by exposing MLE-12 cells to LPS, thereby simulating the pathological conditions associated with ALI. Furthermore, our findings revealed that the decrease in cellular viability caused by LPS exposure was markedly alleviated following VDPS administration, indicating its protective effect against LPS-induced cytotoxicity ($p < 0.05$) (Fig. 5A). Subsequently, we examined whether pretreatment with VDPS or Fer-1 could mitigate oxidative injury induced by LPS exposure. The results showed that cells receiving VDPS or Fer-1 pretreatment exhibited a pronounced reduction in intracellular MDA levels relative to those in the LPS-treated group, suggesting a marked attenuation of lipid peroxidation and oxidative stress ($p < 0.001$) (Fig. 5B). Meanwhile, treatment with VDPS and Fer-1 effectively reinstated the GSH levels that had been markedly diminished following LPS stimulation, indicating their capacity to restore intracellular redox balance ($p < 0.05$) (Fig. 5C). In addition, our results demonstrated that pretreatment with VDPS or Fer-1 markedly attenuated the excessive generation of ROS induced by LPS exposure in MLE-12 cells, thereby alleviating oxidative stress at the cellular level ($p < 0.001$) (Fig. 5F,H). Fer-1 and VDPS pretreatment also significantly suppressed LPS-triggered inflammatory responses, markedly reducing levels of TNF-$\alpha$, IL-1$\beta$, and IL-6 ($p < 0.001$) (Fig. 5D,E,G).

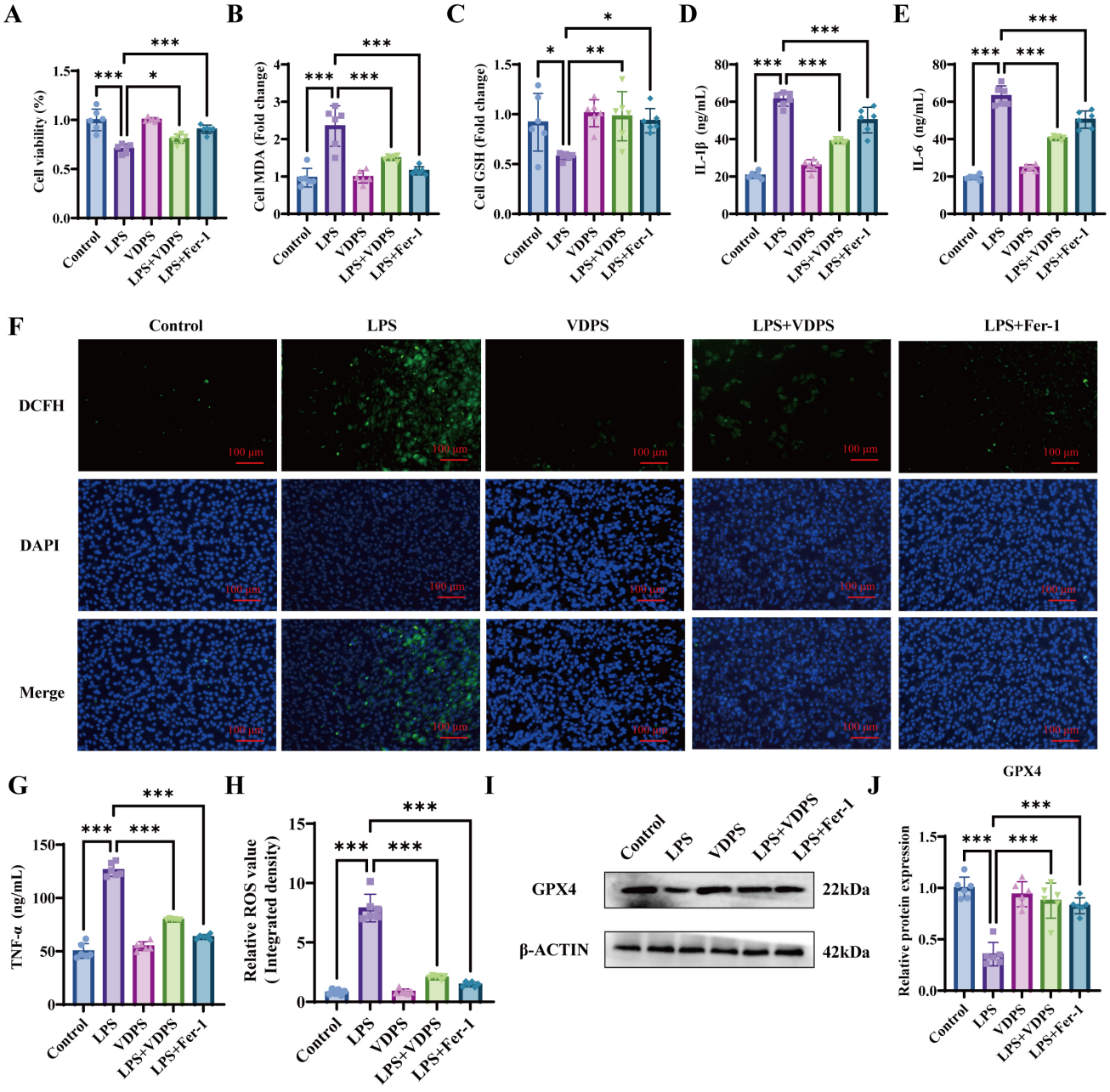


**Fig. 5. VDPS inhibits lipid peroxidation and ferroptosis in MLE-12 cells.** (A) Cell viability of MLE-12 cells under different treatments. (B) MDA content in MLE-12 cells under different treatments. (C) GSH levels in MLE-12 cells under different treatments. (D,E,G) Levels of IL-1$\beta$, IL-6, and TNF-$\alpha$ in cell culture supernatants. (F) ROS content in MLE-12 cells detected by fluorescent probe DCFH-DA; green fluorescence represents ROS (scale bar: 50 μm, magnification 200×). (H) Statistical analysis of ROS in each group. (I) Western blot analysis of GPX4 protein expression. (J) Quantitative analysis of GPX4 protein expression ($n = 6$, *$p < 0.05$, **$p < 0.01$, ***$p < 0.001$). Abbreviations: GSH, Reduced glutathione; GPX4, Glutathione peroxidase 4; IL, Interleukin; LPS, Lipopolysaccharide; MDA, Malondialdehyde; ROS, Reactive oxygen species; TNF-$\alpha$, Tumor necrosis factor alpha.

Subsequently, we observed the effects of VDPS intervention on intracellular GPX4 protein expression. Both VDPS and Fer-1 pretreatment increased GPX4 expression levels, with VDPS pretreatment demonstrating more pronounced ferroptosis resistance ($p < 0.001$) (Fig. 5I,J). These findings suggest that VDPS effectively mitigates LPS-induced ferroptotic injury in MLE-12 cells by suppressing lipid peroxidation and alleviating oxidative damage, thereby contributing to the preservation of cellular integrity and function. These findings indicate that VDPS confers significant protection against LPS-induced ALI by suppressing ferroptosis through multiple coordinated mechanisms. Specifically, VDPS reduces excessive iron accumulation, attenuates lipid peroxidation and inflammatory

signaling, enhances the activity of endogenous antioxidant enzymes, and modulates the expression of key proteins involved in the ferroptotic pathway, thereby collectively maintaining redox balance and cellular homeostasis.

### *MT-1 Enhances the Protective Effect of VDPS on Lung Epithelial Cells and Inhibits Ferroptosis via GPX4 Pathway*

To further investigate whether MT-1 enhances VDPS-mediated protection of lung epithelial cells, we performed LPS stimulation and VDPS treatment following MT-1 knockdown. Experimental observations revealed that, relative to the control group (siCont+LPS+VDPS), silencing of MT-1 expression (siMT-1+LPS+VDPS) led to a marked decline in cellular viability following VDPS administration, indicating that MT-1 may play a crucial role in mediating the cytoprotective effects of VDPS ($p < 0.001$) (Fig. 6A), suggesting that MT-1 deficiency partially inhibited VDPS protective effects on MLE-12 cells. This result indicates that MT-1 presence exerts a sensitizing effect on VDPS antioxidant and anti-oxidative stress functions.

We analyzed intracellular lipid peroxidation levels through classical oxidative stress indicators GSH and MDA. Compared to the siCont+LPS+VDPS group, the siMT-1+LPS+VDPS group showed significantly increased MDA content, markedly reduced GSH levels, and elevated ROS levels, indicating that MT-1 suppression weakened the anti-oxidative stress capacity of VDPS ($p < 0.01$) (Fig. 6B–E). Similarly, compared to the siCont+LPS+VDPS group, the siMT-1+LPS+VDPS group showed markedly higher concentrations of the pro-inflammatory cytokines TNF-$\alpha$, IL-1$\beta$, and IL-6 in the culture supernatants following LPS stimulation, demonstrating that MT-1 silencing effectively abolished the anti-inflammatory effects of VDPS and suggesting that MT-1 is essential for mediating its immunoregulatory activity ($p < 0.01$) (Fig. 6F–H).

To further explore whether MT-1 participates in ferroptosis inhibition by affecting the GPX4 pathway, we analyzed GPX4 protein expression by means of Western blotting. Results showed that compared to the siCont+LPS+VDPS group, the siMT-1+LPS+VDPS group exhibited significantly reduced GPX4 protein levels. This indicates that MT-1 deficiency diminishes VDPS-mediated promotion of GPX4 activity, potentially reducing VDPS inhibitory effects on ferroptosis ($p < 0.001$) (Fig. 6I,J). These results demonstrate that MT-1 and VDPS exert synergistic effects in protecting lung epithelial cells from lipid peroxidation and ferroptosis. MT-1 maintains cellular antioxidant capacity by enhancing VDPS-mediated GPX4 activation, thereby alleviating LPS-induced oxidative damage and ferroptosis.

## Discussion

Previous studies have demonstrated that multiple cell death pathways, including apoptosis [24], autophagy [25], and pyroptosis [26], participate in LPS-induced ALI processes. However, recent ferroptosis research, accompanied by growing understanding of this pathway, has prompted more investigators to explore the relationship between ferroptosis and ALI. Iron ions are considered essential for the ferroptosis process, with excessive iron deposition leading to cellular oxidative stress and membrane lipid peroxidation, ultimately resulting in ferroptotic cell death [7]. Excessive oxidative stress triggers the oxidation of polyunsaturated fatty acids within the lipid bilayer of biological membranes, consequently generating lipid peroxidation by-products such as MDA. This process enhances lipid peroxidation levels in the membrane and ultimately compromises the integrity and stability of the cellular membrane structure [27]. Initially, our observations revealed that the iron concentrations in both lung tissue and serum of mice with LPS-induced ALI were markedly elevated compared to control animals, indicating the presence of dysregulated iron metabolism associated with ALI. Subsequently, in the ALI mouse model, LPS and LPS+Erastin groups showed exacerbated alveolar inflammation and pulmonary edema with increased inflammatory mediator expression, while these manifestations were reversed by Fer-1. Furthermore, our experimental results demonstrated that LPS-induced ALI in mice was accompanied by a pronounced reduction in GSH levels and a substantial elevation in MDA levels within both lung tissue and pulmonary epithelial cells, reflecting heightened oxidative stress and lipid peroxidation. These alterations in iron homeostasis and oxidative stress markers were effectively reversed upon Fer-1 administration, highlighting the pivotal role of oxidative stress in the pathogenesis of LPS-induced ALI.

Ferroptosis can be triggered by various factors involving different signaling pathways, but all upstream pathways ultimately affect glutathione peroxidase activity directly or indirectly, reducing cellular antioxidant capacity and leading to ferroptosis [28,29]. GPX4 serves as the principal enzyme responsible for catalyzing the reduction of phospholipid hydroperoxides (PL-OOH) in mammalian cells. During this process, GPX4 utilizes GSH as a substrate, converting it to its oxidized form while simultaneously reducing the cytotoxic PL-OOH molecules to their corresponding non-toxic lipid alcohols, thereby protecting cells from oxidative damage. Therefore, GPX4 activity inhibition can lead to lipid peroxide accumulation, resulting in ferroptosis [30]. Our study found that GPX4 expression levels in lung tissue and alveolar epithelial cells of LPS-treated mice were lower than controls, with a more pronounced reduction following erastin intervention, while Fer-1 treatment upregulated GPX4 levels in mouse lung tissue and epithelial cells. These results reveal that LPS-induced lung injury triggers

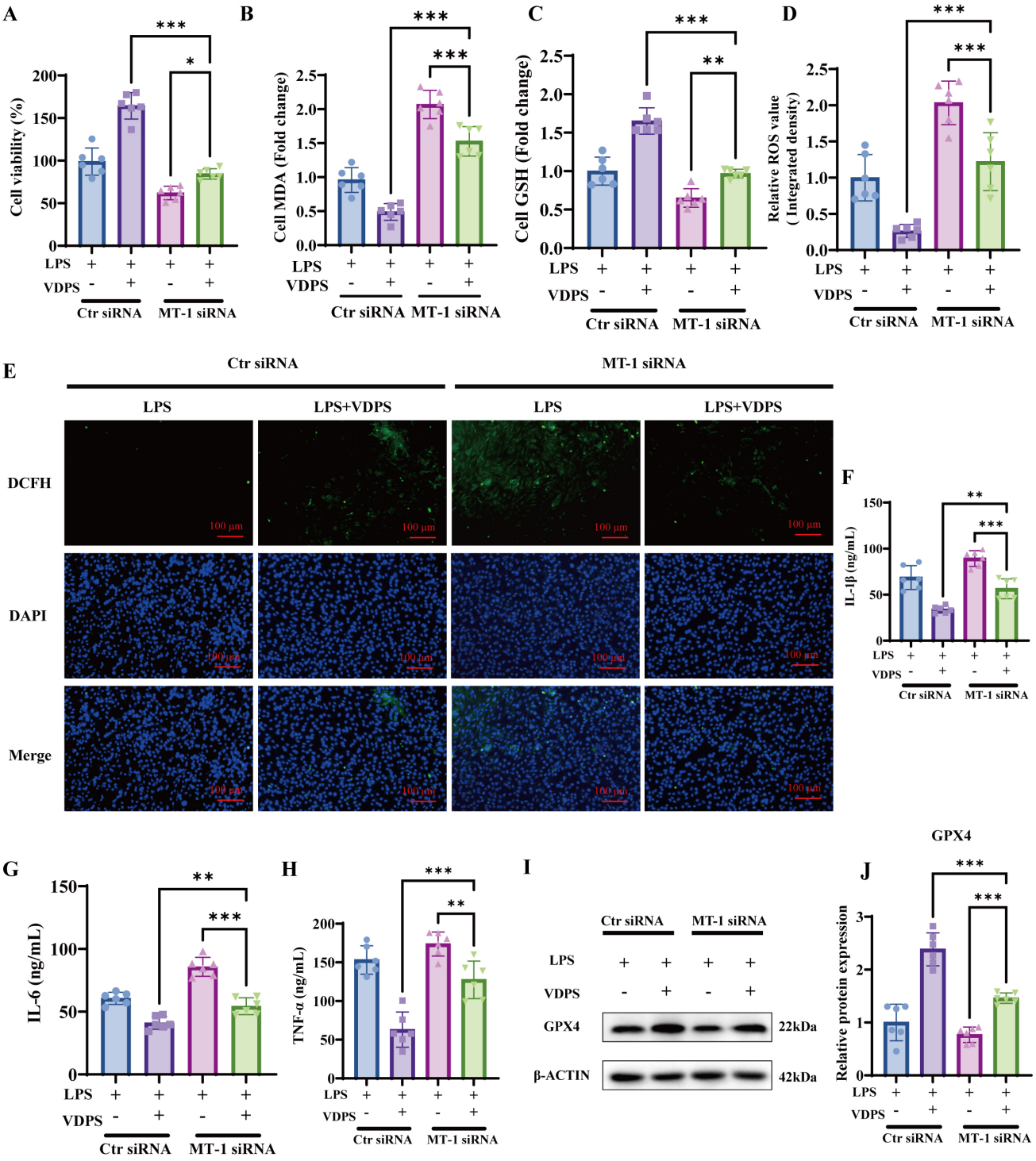


**Fig. 6. MT-1 promotes the protective effect of VDPS on lung epithelial cells and contributes to GPX4-mediated inhibition of ferroptosis.** (A) Cell viability of MLE-12 cells under different treatments. (B) MDA content in MLE-12 cells under different treatments. (C) GSH levels in MLE-12 cells under different treatments. (D) Statistical analysis of ROS in each group. (E) ROS content in MLE-12 cells detected by fluorescent probe DCFH-DA; green fluorescence represents ROS (scale bar: 50 μm, magnification 200×). (F–H) IL-1$\beta$,IL-6, and TNF-$\alpha$ content in cell culture supernatants. (I) Western blot analysis of GPX4 protein expression. (J) Quantitative analysis of GPX4 protein expression ($n = 6$, *$p < 0.05$, **$p < 0.01$, ***$p < 0.001$). Abbreviations: GSH, Reduced glutathione; GPX4, Glutathione peroxidase 4; IL, Interleukin; LPS, Lipopolysaccharide; MDA, Malondialdehyde; ROS, Reactive oxygen species; TNF-$\alpha$, Tumor necrosis factor alpha.

ferroptosis, with the reversal of experimental outcomes by ferroptosis inhibitors further confirming our conclusions.

MT-1 belongs to a family of cysteine-rich, low-molecular-weight proteins with high metal-binding capacity. These proteins are critically involved in various inflammatory conditions, playing key roles in regulating inflammatory responses and modulating immune processes [15]. When bound to metal ions *in vivo*, MT-1 participates in crucial functions including metal ion transport and storage, ROS scavenging, maintenance of intracellular oxidation-reduction balance, autophagy regulation, and apoptosis inhibition. Nevertheless, the specific regulatory function of MT-1 in the progression of ALI remains poorly understood. In the initial phase of our study, bioinformatics analyses were employed to identify MT-1 as a potential biomarker associated with ferroptosis, suggesting its possible involvement in ALI pathophysiology. To further investigate the regulatory relationship between MT-1 and ferroptosis in LPS-stimulated MLE-12 cell injury models, we used liposome transfection to mediate *MT-1* gene knockdown in MLE-12 cells. Research results demonstrated that MT-1 knockdown increased intracellular oxidative stress levels, manifested by significantly elevated MDA and ROS levels in MLE-12 cells, as well as marked reductions in GSH levels and cell viability, suggesting that MT-1 knockdown increases lipid peroxides and oxidative stress levels in lung epithelial cells. The cystine/glutamate antiporter system $Xc^-$-glutathione-GPX4 regulatory axis represents a key regulatory mechanism in ferroptosis control. SLC7A11 induces GSH synthesis by promoting cellular cystine reduction to cysteine [31,32]. Our experimental results demonstrated that silencing MT-1 expression markedly decreased the levels of GPX4 and SLC7A11, thereby promoting ferroptotic cell death and aggravating lung tissue injury. Our findings demonstrate for the first time that MT-1 alleviates LPS-induced ALI by activating the SLC7A11-GSH-GPX4 axis to inhibit ferroptosis, providing a novel molecular mechanism for disease treatment.

A previous study has shown that VDPS alleviates LPS-induced ALI by inhibiting P-selectin–mediated cell adhesion, thereby reducing inflammatory cell recruitment and pulmonary tissue damage [21]. Nevertheless, its specific molecular mechanisms in treating ALI have not been fully elucidated. Our study confirmed that administration of VDPS substantially ameliorated LPS-induced pathological damage in lung tissue and alleviated the severity of pulmonary edema. This protective effect was accompanied by significant reductions in the expression of pro-inflammatory cytokines within the lungs, including IL-1$\beta$, IL-6, and TNF-$\alpha$, indicating effective suppression of the inflammatory response. Cellular susceptibility to ferroptosis is predominantly governed by the balance between ROS accumulation and the activity of GPX4, which together determine the extent of lipid peroxidation and ferroptotic cell death [33], with GPX4 converting toxic lipid ROS to non-toxic lipid alcohols in the presence of GSH, thereby preventing ferroptosis [34,35]. Our research results confirmed that VDPS and Fer-1 treatment reduced excessive lipid ROS accumulation and MDA formation in LPS-induced lung tissue and epithelial cells while increasing GSH production. Furthermore, from a mechanistic perspective, our results demonstrated that VDPS is capable of suppressing GPX4-dependent lipid peroxidation. Based on these observations, VDPS can be regarded as a potent and safe protective agent that effectively inhibits LPS-induced ferroptosis and excessive ROS generation in both *in vivo* and *in vitro* models.

MT-1 has emerged as a context-dependent modulator in inflammatory and oxidative stress-related pathologies. Environmental toxicants such as black carbon and cadmium can markedly induce MT-1 expression in lung epithelial cells, where it mitigates metal-induced oxidative damage and apoptosis [36]. In addition, MT-1 is closely associated with inflammatory regulation, as its elevated expression correlates with increased levels of pro-inflammatory cytokines and enhanced immune activation [15,37]. These results indicate that MT-1 functions as a molecular mediator connecting oxidative damage with inflammatory responses, highlighting its pivotal role in coordinating cellular stress and immune signaling, thereby maintaining cellular homeostasis under stress conditions. Through further exploration, we discovered that MT-1 exerts a sensitizing effect on VDPS. MT-1 can promote VDPS protective effects on lung epithelial cells and reduce oxidative stress levels. Mechanistically, MT-1 interacts with VDPS to increase GPX4 protein expression, thereby exerting ferroptosis-inhibiting functions and ultimately alleviating LPS-induced ALI. However, several limitations of this study should be acknowledged. First, despite the confirmation of ferroptosis involvement in ALI, the underlying mechanism proposed here remains to be fully delineated, as the synergistic interaction between MT-1 and VDPS requires further mechanistic clarification. Second, the experimental design included only MLE-12 cells and lacked additional lung epithelial or endothelial cell models, limiting the generalizability of the findings. Third, the sample size in both *in vivo* and *in vitro* experiments was relatively small, which may affect the statistical robustness. Fourth, VDPS is a complex polysaccharide mixture, and the specific active component or structural domain responsible for the observed effects remains unclear. Fifth, the study did not include comprehensive control groups, such as blank or positive drug controls, which may limit the interpretation of VDPS and MT-1 effects. Finally, the clinical translation of MT-1 or VDPS was not addressed; issues such as feasibility, safety, pharmacokinetics, and potential off-target effects in humans remain to be explored. Future studies with larger sample sizes, diverse cell models, purified active components of VDPS, and more rigorous experimental

designs will be essential to validate these findings and to explore the potential clinical applications of MT-1 and VDPS in ALI.

## Conclusion

In summary, our study demonstrates that MT-1 mitigates LPS-induced ALI by activating the SLC7A11-GSH-GPX4 signaling axis, thereby suppressing ferroptotic cell death. Additionally, VDPS exerts protective effects against LPS-induced ALI by inhibiting ferroptosis through multiple interconnected mechanisms, including the reduction of iron accumulation, attenuation of lipid peroxidation, enhancement of antioxidant enzyme activity, and modulation of the expression of key ferroptosis-related proteins, collectively contributing to the preservation of pulmonary tissue integrity and function. Moreover, this work demonstrates that MT-1 and VDPS exert synergistic protective effects against lipid peroxidation and ferroptosis in lung epithelial cells, suggesting a novel molecular basis for therapeutic development.

## Availability of Data and Materials

The data that support the findings of this study are available from the corresponding author upon reasonable request.

## Author Contributions

NFD: Conceptualization, Methodology, Investigation, Data curation, Funding acquisition, Writing – original draft. NFC: Formal analysis, Validation, Visualization, Writing – review & editing. XFP: Software, Data analysis, Writing – review & editing. MGC: Methodology, Writing – review & editing. TWW: Data curation, Resources, Writing – review & editing. KL: Conceptualization, Supervision, Writing – review & editing. All authors made substantial contributions to the work, reviewed and approved the final manuscript, and agreed to be accountable for all aspects of the work, ensuring that any questions related to the accuracy or integrity of any part of the work are appropriately investigated and resolved.

## Ethics Approval and Consent to Participate

All animal experiments were approved by the Animal Ethics Committee of South Zhejiang Institute of Radiation Medicine and Nuclear Technology Applications (Approval No. ZFY20250362) and were conducted in accordance with institutional guidelines and the international standards for the ethical care and use of animals.

## Acknowledgment

The authors sincerely acknowledge the South Zhejiang Institute of Radiation Medicine and Nuclear Technology Applications for providing the experimental facilities and for granting approval for the animal experiments. Their support and cooperation were essential for the completion of this study.

## Funding

This work was supported by the Zhejiang Provincial Traditional Chinese Medicine Science and Technology Project (Grant No. 2025ZX026).

## Conflict of Interest

The authors declare no conflict of interest.

## References

[1] Meyer NJ, Gattinoni L, Calfee CS. Acute respiratory distress syndrome. Lancet (London, England). 2021; 398: 622–637. https://doi.org/10.1016/S0140-6736(21)00439-6.

[2] Bos LDJ, Ware LB. Acute respiratory distress syndrome: causes, pathophysiology, and phenotypes. Lancet (London, England). 2022; 400: 1145–1156. https://doi.org/10.1016/S0140-6736(22)01485-4.

[3] Long ME, Mallampalli RK, Horowitz JC. Pathogenesis of pneumonia and acute lung injury. Clinical Science (London, England: 1979). 2022; 136: 747–769. https://doi.org/10.1042/CS20210879.

[4] Kumar V. Pulmonary Innate Immune Response Determines the Outcome of Inflammation During Pneumonia and Sepsis-Associated Acute Lung Injury. Frontiers in Immunology. 2020; 11: 1722. https://doi.org/10.3389/fimmu.2020.01722.

[5] Wheeler AP, Bernard GR. Acute lung injury and the acute respiratory distress syndrome: A clinical review. Lancet (London, England). 2007; 369: 1553–1564. https://doi.org/10.1016/S0140-6736(07)60604-7.

[6] Fan E, Brodie D, Slutsky AS. Acute Respiratory Distress Syndrome: Advances in Diagnosis and Treatment. JAMA. 2018; 319: 698–710. https://doi.org/10.1001/jama.2017.21907.

[7] Chen X, Yu C, Kang R, Kroemer G, Tang D. Cellular degradation systems in ferroptosis. Cell Death and Differentiation. 2021; 28: 1135–1148. https://doi.org/10.1038/s41418-020-00728-1.

[8] Wu D, Spencer CB, Ortoga L, Zhang H, Miao C. Histone lactylation-regulated METTL3 promotes ferroptosis via m6A-modification on ACSL4 in sepsis-associated lung injury. Redox biology. 2024; 74: 103194. https://doi.org/10.1016/j.redox.2024.103194.

[9] Pei Z, Qin Y, Fu X, Yang F, Huo F, Liang X, *et al*. Inhibition of ferroptosis and iron accumulation alleviates pulmonary fibrosis in a bleomycin model. Redox Biology. 2022; 57: 102509. https://doi.org/10.1016/j.redox.2022.102509.

[10] Yang L, Cao LM, Zhang XJ, Chu B. Targeting ferroptosis as a vulnerability in pulmonary diseases. Cell Death & Disease. 2022; 13: 649. https://doi.org/10.1038/s41419-022-05070-7.

[11] Ma L, Chen C, Zhao C, Li T, Ma L, Jiang J, *et al*. Targeting carnitine palmitoyl transferase 1A (CPT1A) induces ferroptosis and synergizes with immunotherapy in lung cancer. Signal Transduction and Targeted Therapy. 2024; 9: 64. https://doi.org/10.1038/s41392-024-01772-w.

[12] Liu P, Feng Y, Li H, Chen X, Wang G, Xu S, *et al*. Ferrostatin-1 alleviates lipopolysaccharide-induced acute lung injury via inhibiting ferroptosis. Cellular & Molecular Biology Letters. 2020; 25: 10. https://doi.org/10.1186/s11658-020-00205-0.

[13] Dai H, Wang L, Li L, Huang Z, Ye L. Metallothionein 1: A New Spotlight on Inflammatory Diseases. Frontiers in Immunology. 2021; 12: 739918. https://doi.org/10.3389/fimmu.2021.739918.

[14] Yılmaz S, Kılıç N, Kaya Ş, Taşcı G. A Potential Biomarker for Predicting Schizophrenia: Metallothionein-1. Biomedicines. 2023; 11: 590. https://doi.org/10.3390/biomedicines11020590.

[15] Liu Y, Wu Z, Guo K, Zhou Y, Xing K, Zheng J, *et al*. Metallothionein-1 gene from Exopalaemon carinicauda and its response to heavy metal ions challenge. Marine Pollution Bulletin. 2022; 175: 113324. https://doi.org/10.1016/j.marpolbul.2022.113324.

[16] Weiselberg J, Niu M, Hernandez CA, Fox HS, Calderon TM, Berman JW. Methamphetamine Induces Metallothionein 1 Expression and an Inflammatory Phenotype in Primary Human HIV-Infected Macrophages. International Journal of Molecular Sciences. 2025; 26: 8875. https://doi.org/10.3390/ijms26188875.

[17] Dai B, Liu X, Du M, Xie S, Dou L, Mi X, *et al*. LATS1 inhibitor and zinc supplement synergistically ameliorates contrast-induced acute kidney injury: Induction of Metallothionein-1 and suppression of tubular ferroptosis. Free Radical Biology & Medicine. 2024; 223: 42–52. https://doi.org/10.1016/j.freeradbiomed.2024.07.019.

[18] Zhang W, Luo M, Xiong B, Liu X. Upregulation of Metallothionein 1 G (MT1G) Negatively Regulates Ferroptosis in Clear Cell Renal Cell Carcinoma by Reducing Glutathione Consumption. Journal of Oncology. 2022; 2022: 4000617. https://doi.org/10.1155/2022/4000617.

[19] Wessels I, Pupke JT, von Trotha KT, Gombert A, Himmelsbach A, Fischer HJ, *et al*. Zinc supplementation ameliorates lung injury by reducing neutrophil recruitment and activity. Thorax. 2020; 75: 253–261. https://doi.org/10.1136/thoraxjnl-2019-213357.

[20] Dai JJ, Tao HM, Min QX, Zhu QH. Anti-hepatitis B virus activities of friedelolactones from Viola diffusa Ging. Phytomedicine: International Journal of Phytotherapy and Phytopharmacology. 2015; 22: 724–729. https://doi.org/10.1016/j.phymed.2015.05.001.

[21] Dai N, Li G, Ni J, Li F, Tong H, Liu Y. A novel galactoxylan derived from Viola diffusa alleviates LPS-induced acute lung injury via antagonizing P-selectin-mediated adhesion function. International Journal of Biological Macromolecules. 2023; 242: 124821. https://doi.org/10.1016/j.ijbiomac.2023.124821.

[22] Li J, Li Y, Chen G, Liang Y, Xie J, Zhang S, *et al*. GLUT1 Promotes NLRP3 Inflammasome Activation of Airway Epithelium in Lipopolysaccharide-Induced Acute Lung Injury. The American Journal of Pathology. 2024; 194: 1185–1196. https://doi.org/10.1016/j.ajpath.2024.03.003.

[23] Matute-Bello G, Downey G, Moore BB, Groshong SD, Matthay MA, Slutsky AS, *et al*. An official American Thoracic Society workshop report: Features and measurements of experimental acute lung injury in animals. American Journal of Respiratory Cell and Molecular Biology. 2011; 44: 725–738. https://doi.org/10.1165/rcmb.2009-0210ST.

[24] Tian Y, Zhu CL, Li P, Li HR, Liu Q, Deng XM, *et al*. Nicotinamide Mononucleotide Attenuates LPS-Induced Acute Lung Injury With Anti-Inflammatory, Anti-Oxidative and Anti-Apoptotic Effects. The Journal of Surgical Research. 2023; 283: 9–18. https://doi.org/10.1016/j.jss.2022.09.030.

[25] Shen Y, He Y, Pan Y, Liu L, Liu Y, Jia J. Role and mechanisms of autophagy, ferroptosis, and pyroptosis in sepsis-induced acute lung injury. Frontiers in Pharmacology. 2024; 15: 1415145. https://doi.org/10.3389/fphar.2024.1415145.

[26] Liu C, Zhou Y, Tu Q, Yao L, Li J, Yang Z. Alpha-linolenic acid pretreatment alleviates NETs-induced alveolar macrophage pyroptosis by inhibiting pyrin inflammasome activation in a mouse model of sepsis-induced ALI/ARDS. Frontiers in Immunology. 2023; 14: 1146612. https://doi.org/10.3389/fimmu.2023.1146612.

[27] Su LJ, Zhang JH, Gomez H, Murugan R, Hong X, Xu D, *et al*. Reactive Oxygen Species-Induced Lipid Peroxidation in Apoptosis, Autophagy, and Ferroptosis. Oxidative Medicine and Cellular Longevity. 2019; 2019: 5080843. https://doi.org/10.1155/2019/5080843.

[28] Chen Y, Fang ZM, Yi X, Wei X, Jiang DS. The interaction between ferroptosis and inflammatory signaling pathways. Cell Death & Disease. 2023; 14: 205. https://doi.org/10.1038/s41419-023-05716-0.

[29] Liu J, Kang R, Tang D. Signaling pathways and defense mechanisms of ferroptosis. The FEBS Journal. 2022; 289: 7038–7050. https://doi.org/10.1111/febs.16059.

[30] Zhang W, Liu Y, Liao Y, Zhu C, Zou Z. GPX4, ferroptosis, and diseases. Biomedicine & Pharmacotherapy = Biomedecine & Pharmacotherapie. 2024; 174: 116512. https://doi.org/10.1016/j.biopha.2024.116512.

[31] Koppula P, Zhuang L, Gan B. Cystine transporter SLC7A11/xCT in cancer: Ferroptosis, nutrient dependency, and cancer therapy. Protein & Cell. 2021; 12: 599–620. https://doi.org/10.1007/s13238-020-00789-5.

[32] Shen L, Zhang J, Zheng Z, Yang F, Liu S, Wu Y, *et al*. PHGDH Inhibits Ferroptosis and Promotes Malignant Progression by Upregulating SLC7A11 in Bladder Cancer. International Journal of Biological Sciences. 2022; 18: 5459–5474. https://doi.org/10.7150/ijbs.74546.

[33] Xue Q, Yan D, Chen X, Li X, Kang R, Klionsky DJ, *et al*. Copper-dependent autophagic degradation of GPX4 drives ferroptosis. Autophagy. 2023; 19: 1982–1996. https://doi.org/10.1080/15548627.2023.2165323.

[34] Chen C, Wang D, Yu Y, Zhao T, Min N, Wu Y, *et al*. Legumain promotes tubular ferroptosis by facilitating chaperone-mediated autophagy of GPX4 in AKI. Cell Death & Disease. 2021; 12: 65. https://doi.org/10.1038/s41419-020-03362-4.

[35] He R, Wei Y, Peng Z, Yang J, Zhou Z, Li A, *et al*. $\alpha$-Ketoglutarate alleviates osteoarthritis by inhibiting ferroptosis via the ETV4/SLC7A11/GPX4 signaling pathway. Cellular & Molecular Biology Letters. 2024; 29: 88. https://doi.org/10.1186/s11658-024-00605-6.

[36] Wang L, Bao S, Liu X, Wang F, Zhang J, Dang P, *et al*. Low-dose exposure to black carbon significantly increase lung injury of cadmium by promoting cellular apoptosis. Ecotoxicology and Environmental Safety. 2021; 224: 112703. https://doi.org/10.1016/j.ecoenv.2021.112703.

[37] Jadaun MS, Singh P, Gupta S. Agonism of MT_1 and MT_2 Receptor Mitigates Oxidative Insult, Neuroinflammation, and Cerebral Injury in Cadmium Chloride Treated Animals. Neurochemical Research. 2025; 50: 193. https://doi.org/10.1007/s11064-025-04451-6.